CrossMark

An Extension of the Stefan-Type Solution Method Applicable to Multi-component, Multi-phase 1D Systems

K. C. Lewis[1] · Samuel Coakley[2] · Sean Miele[1]

Abstract We present an extension of the Stefan-type solution method applicable to multi-component, multi-phase 1D porous flows, and illustrate the method by applying it to phase separation dynamics in an NaCl–H_2O-saturated hydrothermal heat pipe. For this example, three mathematical models are constructed. The first two models concern the rate of progression of two interfaces, one separating brine from two-phase fluid and another separating two-phase fluid from single-phase liquid at seawater salinity. The brine layer model shows that the layer may reach quasi-steady-state thickness even while the salt content of the layer continues to increase; the two-phase layer model shows how variable heat flux at the top of the layer leads to departure from the linear growth rate predicted by a simpler model. The third model concerns the temperature profile in the entire column. The governing advection–diffusion equation has highly variable coefficients, with no negligible terms in it in the region of parameter space considered. We present a method to solve this type of equation by constructing a propagator and a corresponding Green's function. Finally, we show how to use the developed framework to test the internal consistency of numerical simulations, again using the 1D heat pipe as an example.

Keywords Heat pipe · Hydrothermal systems · Stefan problem · Analytic solutions

List of symbols

A	Cross-sectional area (m^2)
C	$\frac{\tilde{\sigma} q y_{12}^2}{2A\rho_1 X_1}$ ($m^{-1}\,s^{-1}$)
c	Specific heat (J/kg °C)
$\mathcal{C}$	Content density [(kg or J)/m^3]

✉ K. C. Lewis
klewis@monmouth.edu

[1] Monmouth University, West Long Branch, NJ, USA

[2] Rutgers University, Edison, NJ, USA

$\mathcal{F}$	Mass or heat flux [(kg or J)/m^2 s]
F	$-\mathcal{F}_0/\tilde{\lambda}$ (°C/m)
h	Enthalpy (J/kg)
I	Layer energy or solute content (J or kg)
$\mathbb{N}$	{0, 1, 2, ...} (dimensionless)
Q	Lateral salt loss (kg)
q	Proportionality constant [kg/(m^3 s)]
T	Temperature (°C)
T_{ij}	Temperature of interface between zones i and j (°C)
T_H	Top boundary temperature (°C)
t	Time (s)
v	Darcy volumetric flux (m/s)
X	Bulk salinity (mass fraction)
y	Height (m)
y_{ij}	Position of interface between zones i and j (m)
$y_{12,\infty}$	Quasi-steady brine layer thickness (m)
y_H	Height of the system (m)
Y	$y - y_{23}$ (m)
α	$\frac{\frac{\mathrm{d}}{\mathrm{d}t}\langle\mathcal{C}\rangle}{(\langle\mathcal{C}\rangle - \mathcal{C}_{23})}$ (s^{-1})
β	$\frac{\mathcal{F}}{(\langle\mathcal{C}\rangle - \mathcal{C}_{23})}$ (m/s)
γ	v_l/ϕ (m/s)
Δx	Width of pipe front (m)
Δz	Width of pipe side (m)
$\Delta\sigma$	Exposed surface area (m^2)
ϵ	$C\gamma/\eta^2$ (dimensionless)
ζ	y/y_{23} (dimensionless)
η	$\frac{1}{\xi}\langle\frac{\partial\xi}{\partial t}\rangle$ (s^{-1})
θ	$\theta_\mathrm{I} + \theta_\mathrm{H} = [T - T_{23} - F(y_{23} - y)]/Fy_{23}$ (dimensionless)
θ_H	Solution to homogeneous problem (dimensionless)
θ_I	Solution to inhomogeneous problem (dimensionless)
κ	Thermal diffusivity (m^2/s)
$\tilde{\lambda}$	Medium thermal conductivity (W/m °C)
ξ	ρX (kg/m^3)
ρ	Bulk density (kg/m^3)
$\tilde{\sigma}$	Pipe circumference (m)
τ	$\kappa t/y_{23}^2$ (dimensionless)
ϕ	Porosity (dimensionless)

1 Introduction

In the classical Stefan problem, the half plane ($y \leq 0$) filled with ice is heated from above (i.e., at $y = 0$) and a melt zone propagates downward (Carslaw and Jaeger 1959). The interface between the ice and melt zone separates regions with distinctly different physical properties, which leads to the idea of dividing the system into domains above and below the interface, solving the governing partial differential equation in the two domains separately, and joining the solutions together at the moving interface. An important piece of the problem

is to find the equation governing the rate of interface propagation. We refer to any problem involving at least one moving interface separating regions of distinct physical properties as a "Stefan-type" problem; in this study, we present an extension of the method applicable to 1D problems involving one or more interfaces and whose governing equations may have strongly variable coefficients. We first derive the general framework and then illustrate it by applying it to the 1D hydrothermal saltwater heat pipe. Although this paper focuses on application to the heat pipe, the framework presented generalizes techniques used in early work on the degradation of a column of permafrost (Lewis et al. 2012) and on the expansion of subsurface damage zones in geothermal applications (Lewis et al. 2013). We also note that if a 3D problem can be reduced to a formally 1D problem via, e.g., rotational symmetry, the method presented here may still be applicable.

One motivation for studying the saltwater heat pipe is to gain understanding of processes in seafloor hydrothermal systems. Studies of seafloor hydrothermal activity date back to 1979 when the first hydrothermal vent system was discovered at the Galapagos Spreading Center (Corliss et al. 1979). Since then, it has become clear that these systems significantly affect the ocean's overall chemical composition (Elderfield and Schultz 1996), provide the primary energy source for nearby deep-sea ecosystems (Hessler and Kaharl 1995), and factor into the Earth's heat budget by transferring heat from the mantle to the seafloor (Stein and Stein 1995). Hydrothermal systems thus play a key role in deep-sea biology, geophysics, and geochemistry.

The processes occurring in these systems can be complex, and simplified analog models are useful to establish partial understanding, which can later be used to leverage understanding of more realistic behavior (Lewis 2013); these models are also important for testing numerical simulators. One such model is the two-phase saltwater heat pipe mentioned above. The corresponding pure water problem has been thoroughly studied (Straus and Schubert 1981; Preuss 1985; McGuinness 1990, 1996; Young 1996; Xu and Lowell 1998); however, accounting for the presence of salt leads to significant complications. Moreover, accounting for salt is often crucial when modeling high-temperature seafloor hydrothermal flows. For example, one of the key observations from sampling hydrothermal vent fluids is their widely varying salinities, and this fact is most easily accounted for by invoking phase separation (Berndt and Seyfried 1990; Von Damm et al. 1997, 2002; Von Damm 2004). While there have been numerical studies of saltwater heat pipes (Bai et al. 2003; Lewis and Lowell 2009b), there are no analytical studies known to the authors.

Due to the presence of salt, phase separation leads to the formation of three layers in a submarine heat pipe. From the seafloor downward, they are a single-phase liquid region at seawater salinity, a two-phase region containing liquid and vapor, and a layer of brine (Bai et al. 2003; Lewis and Lowell 2009b). After introducing the general framework, we employ it to construct mathematical models giving the positions of the interfaces between these layers as functions of time. The general method involves converting a partial differential equation describing the balance of solute or energy into an ordinary differential equation for the corresponding interface position. After determining the interface positions, we incorporate this information in the form of moving boundary conditions to solve the equation governing energy balance. We then use our results to test the internal consistency of a numerical heat pipe simulation.

2 General Problem and Solution Framework

Consider a 1D column of material whose height is given by y_H and whose energy balance at each point is expressible as

$$\frac{\partial T}{\partial t} - \kappa(y, t)\frac{\partial^2 T}{\partial y^2} = f(y, t), \tag{1}$$

where κ is the thermal diffusivity, f is a function that includes the effects of heat sources or advection, and y is the distance from the bottom of the column to a point within the column (for a derivation, see Carslaw and Jaeger 1959). The boundary and initial conditions are given by

$$T(y_{\mathrm{H}}, t) = T_{\mathrm{H}}, \tag{2}$$

$$\frac{\partial T}{\partial y}(0, t) = F, \tag{3}$$

and

$$T(y, 0) = T_{\mathrm{H}}. \tag{4}$$

We take the bottom boundary condition as one of the constant heat flux, thus imposing a fixed temperature gradient F at $y = 0$. Although we have assumed a flux-type boundary condition at the bottom of the column, the solution method presented below is easily adapted to the case of a constant temperature bottom boundary.

Suppose the solution domain is divided into two distinct regions by an upward moving interface initially located at $y = 0$ and whose propagation speed depends on the transport of heat or solute across that interface. We designate the part of the column below the interface as "region i," the part above as "region j," and the position of the interface itself as y_{ij}. We assume that κ can be regarded as a constant in each region separately, i.e., that it is of the form

$$\kappa(y, t) = (\kappa_i - \kappa_j)H[y_{ij}(t) - y] + \kappa_j, \tag{5}$$

where H is the Heaviside step function. We assume further that, in a given region, the profiles of $f(y, t)$ at different times are similarity transformations of each other; in particular, that

$$f(y, t) = \tilde{f}\left(\frac{y}{y_{ij}(t)}\right) \tag{6}$$

for some function $\tilde{f}$. With these assumptions, Eq. (1) may be solved in each region separately, subject to boundary and initial conditions appropriate for that region, with the temperature required to vary continuously across the interface.

2.1 Interface Position

The position of the interface is governed by the conservation of energy or solute, depending on the nature of the interface under consideration. We apply the balance of either of these quantities to the column shown in Fig. 1. If $\mathcal{C}$ represents the volume density of solute or energy in the expanding layer, then the total content of the layer can be written as

$$I(t) \equiv A \int_0^{y_{ij}(t)} \mathcal{C}(y, t)\mathrm{d}y, \tag{7}$$

where A is the cross-sectional area of the column. If y_{ij} increases by an amount Δy_{ij}, then the expansion zone will contain $\mathcal{C}(y_{ij}, t)\Delta y_{ij} A$ more solute or energy. Also, if the flux $\mathcal{F}_0$ at the bottom of the expansion zone is larger than the flux $\mathcal{F}_{ij}$ at the top, the zone content will

Fig. 1 Interface between regions i and j moves upward, driven by the difference in the fluxes of solute or heat between the top and bottom of the expansion zone. These fluxes are represented by $\mathcal{F}_{ij}$ and $\mathcal{F}_0$. At a given time t, region i is below $y_{ij}(t)$, and region j is above $y_{ij}(t)$
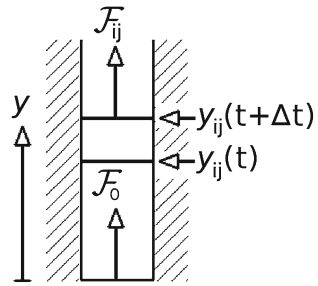
increase by an amount $(\mathcal{F}_0 - \mathcal{F}_{ij})A\Delta t$. Therefore, the increase in the heat or salt content after a time Δt is

$$\Delta I = (\mathcal{F}_0 - \mathcal{F}_{ij})A\Delta t + C(y_{ij}, t)\Delta y_{ij}A. \tag{8}$$

Dividing this equation by $A\Delta t$ and taking the limit as $\Delta t \to 0$ yields

$$\frac{1}{A}\frac{dI}{dt} = \frac{d}{dt}\int_0^{y_{ij}(t)} C(y, t)dy = \mathcal{F} + C(y_{ij}, t)\frac{dy_{ij}}{dt}, \tag{9}$$

where we have defined $\mathcal{F} \equiv \mathcal{F}_0 - \mathcal{F}_{ij}$. Introducing the average content density

$$\langle \mathcal{C} \rangle \equiv \frac{1}{y_{ij}(t)}\int_0^{y_{ij}(t)} C(y, t)dy, \tag{10}$$

Equation (9) can be expressed as

$$\frac{d}{dt}(y_{ij}\langle \mathcal{C} \rangle) = \mathcal{F} + C(y_{ij}, t)\frac{dy_{ij}}{dt}. \tag{11}$$

Using the product rule for differentiation and rearranging gives

$$\frac{dy_{ij}}{dt}(\langle \mathcal{C} \rangle - \mathcal{C}_{ij}) + y_{ij}\frac{d}{dt}\langle \mathcal{C} \rangle = \mathcal{F}, \tag{12}$$

where $\mathcal{C}_{ij} \equiv C(y_{ij}, t)$. By solving this equation in a specific scenario, the interface position as a function of time may be obtained. "Appendix 1" contains an alternative derivation of (12), which has the advantage of being shorter, though perhaps not as physically intuitive as the above derivation. Also, Eq. (12) appears different from the classical "Stefan condition." "Appendix 2" shows how this condition may be derived from (12).

2.2 Column Temperatures

In the region below the interface, Eq. (1) takes the form

$$\frac{\partial T}{\partial t} - \kappa_i\frac{\partial^2 T}{\partial y^2} = \tilde{f}\left(\frac{y}{y_{ij}}\right). \tag{13}$$

The boundary and initial conditions are

$$\frac{\partial T}{\partial y}(0, t) = F, \tag{14}$$

$$T(y_{ij}, t) = T_{ij}, \tag{15}$$

and

$$T(y, 0) = T_{ij}. \tag{16}$$

In Eqs. (15) and (16), T_{ij} is the temperature at $y = y_{ij}$. Although the initial thickness of the region below the interface is zero, condition (16) is still required in order for the governing Eq. (13) to have a unique solution. The problem may be expressed in dimensionless form by introducing the variables

$$\zeta \equiv \frac{y}{y_{ij}}, \tag{17}$$

$$\tau \equiv \frac{\kappa_i t}{y_{ij}^2}, \tag{18}$$

and

$$\theta \equiv \frac{T - T_{ij} - F(y_{ij} - y)}{F y_{ij}}. \tag{19}$$

In the following, we neglect the time dependence of y_{ij} in evaluating $\frac{\partial T}{\partial t}$; this approximation is valid under the condition that

$$\frac{dy_{ij}}{dt} \ll \frac{\kappa_i}{y_{ij}}. \tag{20}$$

This condition is sufficient, though not necessary—see "Appendix 3" for a derivation. The form of the dimensionless temperature $\theta(\zeta, \tau)$ is chosen to make the boundary conditions homogeneous. In terms of these variables, Eq. (1) becomes

$$\frac{\partial \theta}{\partial \tau} - \frac{\partial^2 \theta}{\partial \zeta^2} = \frac{y_{ij}}{F \kappa_i} \tilde{f}(\zeta) \equiv \tilde{g}(\zeta). \tag{21}$$

For now, we assume nothing further about the form of $\tilde{g}(\zeta)$; in Sect. 4.3, however, we consider a specific form for this function. The boundary and initial conditions for the dimensionless problem are

$$\frac{\partial \theta}{\partial \zeta}\bigg|_{\zeta=0} = 0, \tag{22}$$

$$\theta(1, \tau) = 0, \tag{23}$$

and

$$\theta(\zeta, 0) = 1 - \zeta. \tag{24}$$

We solve Eqs. (21) through (24) in two steps. First, we solve the homogeneous problem (with $\tilde{g}(\zeta) = 0$) by constructing an integral operator that propagates the initial temperature distribution $\theta_H(\zeta, 0)$ forward in time to give $\theta_H(\zeta, \tau)$, where the subscript H denotes the solution to the homogeneous problem. Second, we use the propagator to construct a Green's function, which may then be used to solve the inhomogeneous problem, whose solution we represent as $\theta_I(\zeta, \tau)$. The solution $\theta_H(\zeta, \tau)$ satisfies (24), while $\theta_I(\zeta, 0) = 0$; both solutions satisfy (22) and (23). Hence, by linearity the full solution is be given by

$$\theta(\zeta, \tau) = \theta_H(\zeta, \tau) + \theta_I(\zeta, \tau). \tag{25}$$

"Appendix 4" gives the derivations of θ_H and θ_I using the propagator and Green's function formalism; the resulting solutions are

$$\theta_H(\zeta, \tau) = 2 \sum_{n=0}^{\infty} \frac{1}{\lambda_n} e^{-\lambda_n \tau} \cos(\sqrt{\lambda_n} \zeta), \tag{26}$$

and

$$\theta_I(\zeta, \tau) = 2 \sum_{n=0}^{\infty} \frac{1 - e^{-\lambda_n \tau}}{\lambda_n} \cos(\sqrt{\lambda_n} \zeta) \int_0^1 \cos(\sqrt{\lambda_n} \zeta') \tilde{g}(\zeta') d\zeta', \tag{27}$$

where

$$\lambda_n \equiv \left[\frac{(2n + 1)\pi}{2} \right]^2. \tag{28}$$

Solving Eq. (19) for T and reverting back to dimensional variables yields

$$T(y, t) = F y_{ij} \theta \left(\frac{y}{y_{ij}}, \frac{\kappa_i t}{y_{ij}^2} \right) + T_{ij} + F(y_{ij} - y). \tag{29}$$

The solution to the full initial-boundary value problem is given by Eq. (25) through (29).

The temperatures above y_{ij} are the solutions to

$$\frac{\partial T}{\partial t} - \kappa_j \frac{\partial^2 T}{\partial y^2} = \tilde{f} \left(\frac{y}{y_{ij}} \right). \tag{30}$$

with the boundary and initial conditions

$$T(y_{ij}, t) = T_{ij}, \tag{31}$$

$$T(y_H, t) = T_H, \tag{32}$$

and

$$T(y, 0) = T_H. \tag{33}$$

This problem can be solved using the same method as for the region below y_{ij}; the only difference being that, to make the boundary conditions homogeneous, the dimensionless temperature should now be defined as

$$\theta = \frac{T_H - T_S}{T_{ij}}, \tag{34}$$

where

$$T_S = \frac{T_{ij}(y - y_H) + T_H(y_{ij} - y)}{y_{ij} - y_H}. \tag{35}$$

Because the source of solute or heat is at the base of the column, one may find in practice that a simplification is possible for the region $y \geq y_{ij}$, so that the full machinery developed above is not required for this region. Such is the case for the example of the heat pipe.

Fig. 2 In solving for the temperatures inside the heat pipe, we employ the geometry and boundary conditions shown in the above schematic. Q represents the bottom heat flux, T the temperature, B the brine region, L + V the two-phase region, and L the single-phase liquid region. In subscripted variables, these regions will be referred to by numerals 1 through 3. Finally, y_{12} represents the boundary between the B and L + V regions, y_{23} that between the L + V and L regions; y_H is the height of the total system
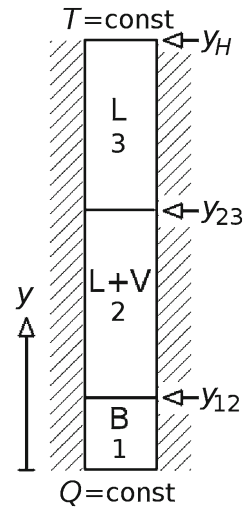
3 Application to the Heat Pipe

Figure 2 shows the geometry and boundary conditions for the heat pipe, modeled as a vertical column of NaCl–H$_2$O-saturated porous material heated from below. No salt, mass, or heat enters through the sides; no salt or mass enters the bottom, to which a constant heat flux is applied. The top boundary of the system is held at constant temperature. Initially, the column contains only single-phase liquid (shown as L). When the temperature at the bottom reaches a critical threshold, a region of two-phase liquid plus vapor (shown as L + V) forms at the bottom of the system and expands upward. Phase separation within this layer gives rise to a layer of brine (shown as B) at the base of the system, which also expands upward with time. A small volume of vapor can be present in this region as well. We seek expressions for the position of the interface between the B and L + V zones (denoted by y_{12}), that of the interface between the L + V and L zones (denoted by y_{23}), and for the temperature throughout the pipe.

3.1 Brine Layer

We now use (12) to derive an equation governing the thickness of the brine layer as a function of time. The volume density of salt in the brine layer is given by

$$\mathcal{C} = \phi \rho X, \tag{36}$$

where ϕ is the porosity, ρ is the bulk density, and X is the bulk salinity. No salt enters or leaves the bottom boundary of the system, so $\mathcal{F}_{bot} = 0$. The flux of salt into the top of the brine layer is approximately

$$\mathcal{F}_{12} \approx (\rho_l v_l X_l)_{12}, \tag{37}$$

where v is the Darcy volumetric flux and the subscript l denotes the liquid phase; we assume that salt carried in the vapor phase and diffusion of salt are both small compared to the amount of salt advected by the liquid (this assumption is verified in Sect. 4.1). Denoting the interface position by y_{12} and substituting these expressions into (12) results in

$$\frac{dy_{12}}{dt} \left[\langle \phi\rho X \rangle - (\phi\rho X)_{12} \right] + y_{12} \frac{d\langle \phi\rho X \rangle}{dt} = (\rho_1 v_1 X_1)_{12}. \tag{38}$$

Taking ϕ as a constant and defining $\xi \equiv \rho X$, the above equation may be written as

$$\frac{dy_{12}}{dt} \left(\langle \xi \rangle - \xi_{12} \right) + y_{12} \frac{d}{dt} \langle \xi \rangle = \left(\xi_1 \frac{v_1}{\phi} \right)_{12}. \tag{39}$$

Dividing both sides by the coefficient of dy_{12}/dt gives

$$\frac{dy_{12}}{dt} + y_{12}\eta = \gamma, \tag{40}$$

where

$$\eta \equiv \frac{1}{(\langle \xi \rangle - \xi_{12})} \frac{d}{dt} \langle \xi \rangle. \tag{41}$$

and

$$\gamma \equiv \frac{1}{(\langle \xi \rangle - \xi_{12})} \left(\xi_1 \frac{v_1}{\phi} \right)_{12}. \tag{42}$$

In Sect. 4.1, we solve Eq. (40) for specific forms of $\gamma(t)$ and $\eta(t)$.

3.2 Two-phase Layer

To derive the position of the interface between the two-phase fluid and overlying single-phase liquid zones, we again employ Eq. (12), this time setting

$$\mathcal{C} = \phi\rho h + (1 - \phi)\rho_r c_{pr} T, \tag{43}$$

where h is the fluid bulk enthalpy, c_p is the specific heat at constant pressure, T is the temperature, and the subscript r refers to the rock phase. We also set

$$\mathcal{F} = \rho_1 h_1 v_1 + \rho_v h_v v_v - \tilde{\lambda} \frac{\partial T}{\partial y}, \tag{44}$$

where $\tilde{\lambda}$ is the effective medium thermal conductivity. Denoting the location of the interface by y_{23}, we write Eq. (12) as

$$\frac{dy_{23}}{dt} + \alpha y_{23} = \beta. \tag{45}$$

where

$$\alpha \equiv \frac{\frac{d}{dt}\langle \mathcal{C} \rangle}{(\langle \mathcal{C} \rangle - \mathcal{C}_{23})} \tag{46}$$

and

$$\beta \equiv \frac{\mathcal{F}}{(\langle \mathcal{C} \rangle - \mathcal{C}_{23})}. \tag{47}$$

We solve this equation and compare the solution with that from a numerical simulation in Sect. 4.2.

3.3 Pipe Temperature

The equation governing energy balance is approximately

$$\frac{\partial}{\partial t}\left[(1-\phi)\rho_r c_{pr} T + \phi\rho h\right] + \frac{\partial}{\partial y}(\rho_l v_l h_l + \rho_v v_v h_v) = \tilde{\lambda}\frac{\partial^2 T}{\partial y^2}. \tag{48}$$

For a derivation of the full equation and a discussion of when terms we have neglected become important, see Stauffer et al. (2014). For present purposes, it is useful to rewrite this equation as

$$(1-\phi)\rho_r c_{pr}\frac{\partial T}{\partial t} + \phi\rho\frac{\partial h}{\partial t} - \tilde{\lambda}\frac{\partial^2 T}{\partial y^2} = -\phi h\frac{\partial\rho}{\partial t} - \frac{\partial}{\partial y}(\rho_l v_l h_l + \rho_v v_v h_v). \tag{49}$$

The time dependence of y_{23} derived above encapsulates the effects of latent heat as single-phase liquid is converted into two-phase liquid and vapor. Moreover, this interface splits the system into two parts, in each of which latent heat effects are negligible. Therefore, we employ the machinery developed in Sect. 2 to solve the energy equation and construct temperature profiles in the regions below and above y_{23} separately. For a discussion of how it can be conceptually useful to split the term involving $\phi\rho h$ and move the density derivative to the right-hand side of (48), see Sect. 5.2.

In the zones below and above y_{23}, we may replace h with $c_p T$, where c_p is the fluid bulk specific heat at constant pressure. Making this replacement on the left-hand side of (49) yields

$$\tilde{\rho}c_p\frac{\partial T}{\partial t} - \tilde{\lambda}\frac{\partial^2 T}{\partial y^2} = -\phi h\frac{\partial\rho}{\partial t} - \frac{\partial}{\partial y}(\rho_l v_l h_l + \rho_v v_v h_v), \tag{50}$$

where we have defined the medium bulk quantity $\tilde{\rho}c_p \equiv (1-\phi)\rho_r c_{pr} + \phi\rho c_p$. Dividing through by $\tilde{\rho}c_p$ and introducing the thermal diffusivity $\kappa \equiv \tilde{\lambda}/\tilde{\rho}c_p$ gives

$$\frac{\partial T}{\partial t} - \kappa\frac{\partial^2 T}{\partial y^2} = -\frac{1}{\tilde{\rho}c_p}\left[\phi h\frac{\partial\rho}{\partial t} + \frac{\partial}{\partial y}(\rho_l v_l h_l + \rho_v v_v h_v)\right] \equiv f(y,t), \tag{51}$$

The governing equation is now written in the form of (1), and the solution for the temperatures below y_{23} is given in Sect. 2.2; we now discuss the temperatures above y_{23} separately. The resulting pipe temperature profile is compared with that from a numerical simulation in Sect. 4.3.

3.4 Temperatures Above y_{23}

The fluid above y_{23} moves upward due to the fact that fluid in the column below is thermally expanding. However, the y_{23} boundary itself moves upward at a rate dy_{23}/dt, which we assume is much greater than the thermal expansion speed of the liquid. It is then convenient to solve the problem in the frame of reference that moves upward in time with the y_{23} interface, and thereafter to revert back to the frame of reference that is at rest with respect to the rock matrix. Defining

$$Y \equiv y - y_{23}, \tag{52}$$

using the approximation $h \approx c_p T$, and keeping in mind that the liquid phase is the only one present, Eq. (51) takes the form

$$\frac{\partial T}{\partial t} - \kappa \frac{\partial^2 T}{\partial Y^2} = -\left(\frac{\phi c_p T}{\widetilde{\rho} c_p}\right) \frac{\partial \rho}{\partial t} + u \frac{\partial T}{\partial Y}, \tag{53}$$

where $u = v - dy_{23}/dt$ is the volumetric flux relative to the moving interface. We assume that the dominant balance in this equation is between the diffusive and advective terms, giving

$$\frac{\partial^2 T}{\partial Y^2} + \frac{u}{\kappa} \frac{\partial T}{\partial Y} = 0, \tag{54}$$

where partial derivatives have been maintained because T depends on time through y_{23}. Solving this equation and reverting back to Earth-frame coordinates leads to

$$T(y, t) = (T_H - T_{23}) \left[\frac{e^{(v - \dot{y}_{23})(y - y_{23})/\kappa} - 1}{e^{(v - \dot{y}_{23})(y_H - y_{23})/\kappa} - 1} \right] + T_{23}. \tag{55}$$

4 Comparison with a Numerical Solution

We now indicate how the solutions generated in the previous sections may be used to investigate the internal consistency of a numerical heat pipe simulation. For this purpose, we use the code FISHES, which was designed by K.C. Lewis (for details, see Lewis and Lowell 2009a, b) and used in many previous studies involving multi-phase, multi-component fluid flow in hydrothermal systems (Choi and Lowell 2015; Lowell et al. 2015; Singh et al. 2013; Han et al. 2013; Steele-MacInnis et al. 2012a, b). The code and a user's manual are available publicly at http://wlb-physics-01.monmouth.edu/fishes.htm.

The geometry and boundary conditions for the simulation are shown in Fig. 3. A 100-m-long vertical, fluid-saturated, porous column is heated from below with a constant flux of 1 W/m^2. The porosity is 0.1, the permeability is 10^{-15} m^2, and the relative permeability of each phase is set equal to the volume saturation of that phase. The bottom is maintained at zero salt and total mass flux. The interior of the pipe is initially at 393 °C and at a salinity of 3.2 wt%NaCl. The temperature is chosen to be near the critical point of NaCl–H$_2$O for the system pressure, which increases hydrostatically starting from a fixed 260 bars at the top boundary. The top boundary has "flow-through" conditions imposed on heat and salinity. The meaning of this condition is as follows: If the fluid velocity at the top boundary is directed out of the system, the temperature and salinity at that boundary are set to those of the computational node directly below; if the fluid velocity is directed into the system, then the salinity is set to 3.2 wt% NaCl while the temperature is set to 393 °C. This type of boundary condition treats the upper boundary as being in contact with an infinite reservoir of fluid above it, having a salinity of 3.2 wt% NaCl and a temperature of 393°C. The system is simulated for 40 years, long enough for the two-phase zone to propagate a significant distance into the system but not so long that it interacts significantly with the top boundary.

Figures 4, 5, and 6 show the results of the simulation. Starting after about 2 years of simulation time, a liquid-plus-vapor region grows from the bottom and has reached 60 meters from the bottom of the system by 40 years. Meanwhile, a layer of brine forms at the bottom of the system, reaching a height of about 2.3 m by 4 years.

Fig. 3 For comparison with the analytic solution, a numerical solution is generated using FISHES, employing the geometry and boundary conditions shown above. The column consists of 100 computational nodes, each with 1 m length except toward the bottom of the system, where the resolution starts at 0.2 m and increases linearly to 1 m over 20 nodes. The meaning of the "flow-through" boundary conditions at the top is addressed in the text

$p=$const
flow-through
heat , salt

100 m

$Q=$const
0 salt flux
0 mass flux
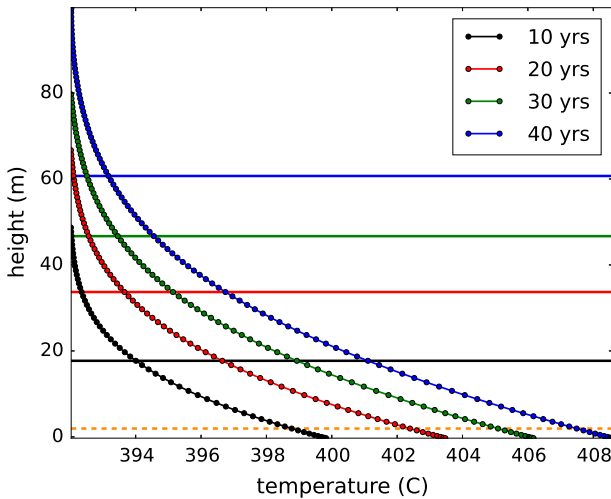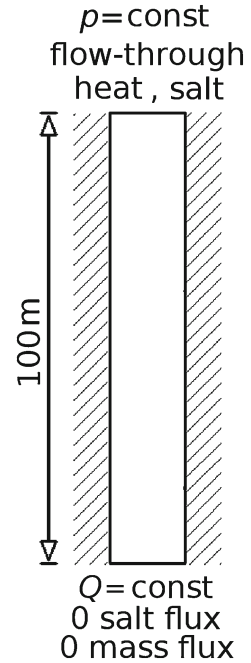
Fig. 4 Dotted curves show temperatures within a heat pipe at times of 10–40 years simulated using the code FISHES. The *orange dashed line* represents the location of the interface between the brine and liquid-plus-vapor layers, which is stable at times >3 years. The *solid black*, *red*, *green*, and *blue horizontal lines* show the location of the interface between the liquid-plus-vapor and single-phase liquid layers
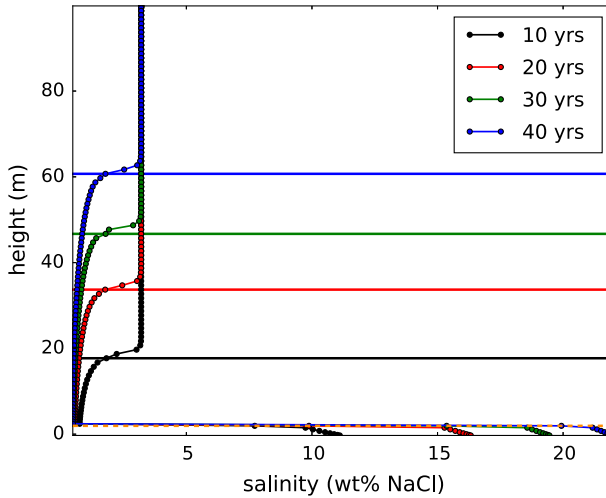
Fig. 5 These system salinities correspond to the same simulation times as in Fig. 4, with *horizontal lines* showing the same interface positions. The interface between the brine region and the liquid-plus-vapor region is defined as the height below which the salinity is greater than 3.2 wt% NaCl (i.e., <5 m). Note that the liquid-plus-vapor region has salinities lower than this value
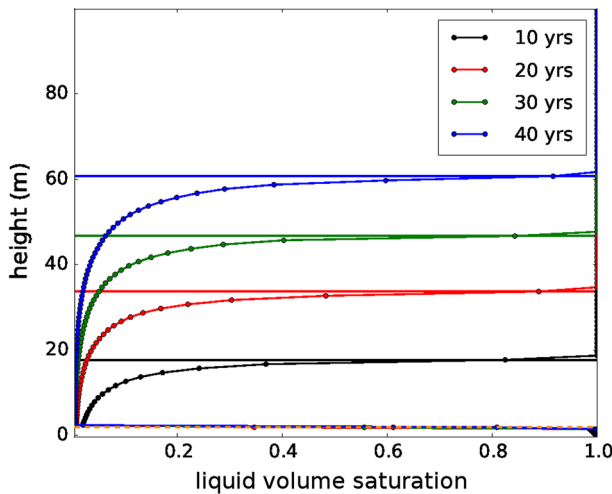
Fig. 6 Three regions have characteristic liquid volume saturations: unity for the single-phase liquid region; much less than unity (on average) for the liquid-plus-vapor region; and just below unity for the brine region. We note, however, that these saturations likely depend strongly on the relative permeability model employed, a linear model in this case (see Sect. 4)
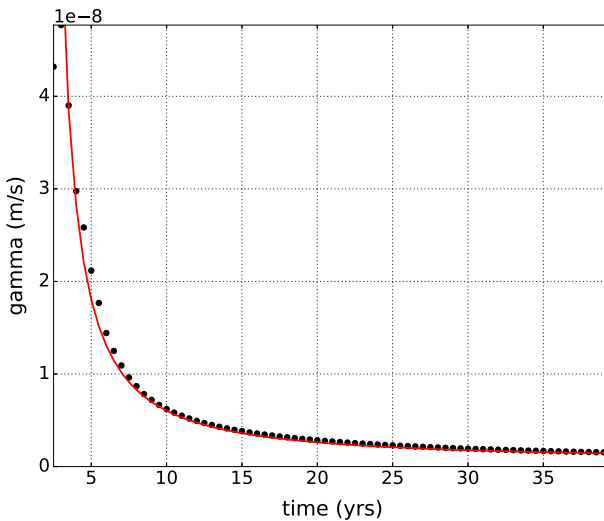
4.1 Brine Layer Model

To compare these results with the brine layer model from Sect. 3.1, we approximate the numerically derived values of $\gamma(t)$ at the top of the brine layer as

$$\gamma(t) = \frac{\gamma_1}{(t - t_{\gamma s})^{5/4}} + \gamma_2, \tag{56}$$

Table 1 Numerically derived constants used in the models of this study

Constant	Value
γ_1	2.198×10^2 m s$^{1/4}$
γ_2	6.0×10^{-10} m/s
$t_{\gamma s}$	4.0×10^{-9} m/s
a	2.26 m
b	3×10^{-8} s^{-1}
$\alpha_{1/2}$	5.63×10^{-10} s^{-1}
β_0	6.8×10^{-8} m/s
S	0.7
n	1/2

Fig. 7 Above values of $\gamma(t)$ were obtained numerically by tracking the interface between the brine and two-phase regions from the FISHES heat pipe simulation. The *red curve* shows the continuous approximation to this curve

where the values of γ_1, γ_2, $t_{\gamma s}$, and all other constants employed in this study are given in Table 1. Figure 7 shows the numerical values of v_1/ϕ together with those given by (56), starting from the time at which the brine layer begins to form. The black dots in Fig. 8 show the simulated brine layer thickness as a function of time; based on this curve, we attempt to solve (40) by assuming a solution of the form

$$y_{12}(t) = a \tanh(bt), \tag{57}$$

where a and b are constants to be determined. Substituting (57) into (40), we find that $\eta(t)$ must have the form

$$\eta(t) = \frac{\gamma(t) - ab \operatorname{sech}^2(bt)}{a \tanh(bt)} \tag{58}$$

for this proposed solution to be successful; this form can be fit to the numerically generated $\eta(t)$ with the values of a and b shown in Table 1 (see Fig. 9). Thus, the numerical forms
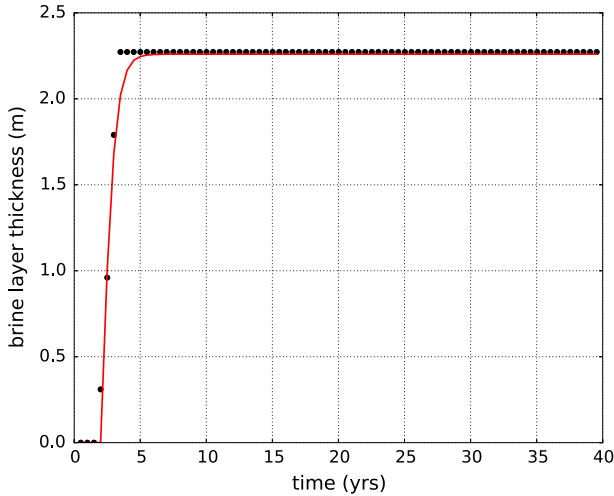
Fig. 8 Solution, $y_{12}(t)$, of Eq. (40) (*solid red curve*) is plotted over the simulated values for the height of the interface between the brine and the overlying two-phase region (*black dots*)
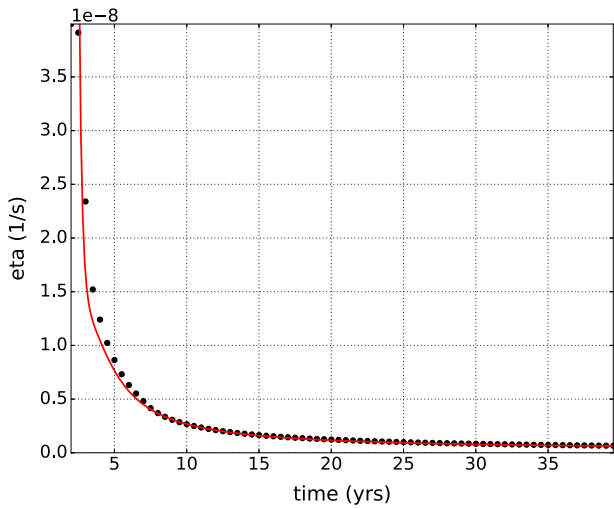
Fig. 9 Numerical values of $\eta(t)$ (*black dots*) are compared with those given by (58) (*solid red curve*) together with the constants a and b from Table 1

for γ and η determine the constants a and b, and the resulting brine layer thicknesses given by (57) are shown in Fig. 8 together with simulated values. Finally, we test the assumption, from Sect. 3.1, that the salt contained in the brine layer is delivered primarily through the liquid-phase advection of salt. Figure 10 shows a comparison between the time-integrated flux of salt through the top of the brine layer, obtained from the numerically derived values of $(\rho_l v_l X_1)_{12}$, and the simulated salt content of the brine layer. This comparison also shows that, for the progression of the brine interface, the second term on the right-hand side of equation (9) is small compared to the first; such is not the case for the interface between the two-phase
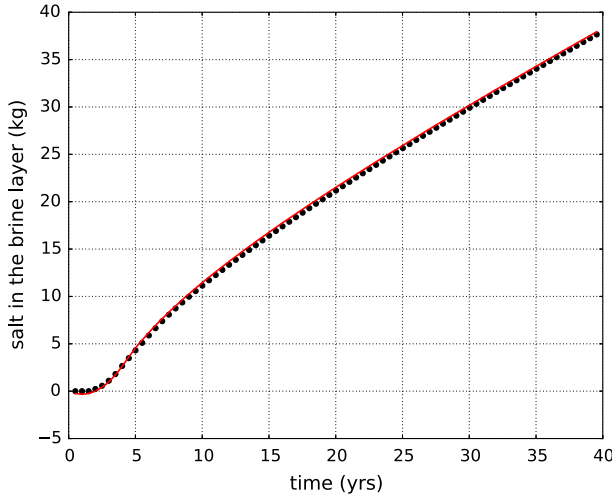
Fig. 10 Simulated values of the amount of salt contained in the brine layer as a function of time (*black dots*), together with those determined by integrating Eq. (37) with respect to time

and single-phase zones; this difference is due to the fact that, contrary to salt transport, heat is transported through the rock phase as well as through the fluid.

4.2 Two-Phase Layer Model

In contrast to the brine layer thickness, the two-phase zone thickness increases throughout the simulation; this property leads to a different shift in the dominant terms of the balance expressed by (45) than was the case for (40). As the initial interface position is $y_{23} = 0$, we assume that, at early times, the dominant balance in equation (45) is between dy_{23}/dt and β. This balance implies that β is the initial speed of propagation of the interface. On the other hand, αy_{23} increases with time while β decreases, so that at late times αy_{23} becomes important. Replacing α and β with initial and mid-simulation values, $\alpha_{1/2}$ and β_0, the solution to equation (45) is given by

$$y_{23}(t) = \frac{\beta_0}{\alpha_{1/2}} \left(1 - e^{-\alpha_{1/2}t} \right). \tag{59}$$

Taking a Taylor series expansion of the exponential term for small times shows that (59) does incorporate an initial interface speed of β_0. Figure 11 compares the solution above with that from the numerical simulation, where the numerically derived values used for $\alpha_{1/2}$ and β_0 appear in Table 1.

4.3 Pipe Temperature Model

Using equation (29) (with $i = 2$ and $j = 3$) and (55), we compare the temperatures predicted by our model with those derived numerically; however, before (29) can be used, a form must be given for the function $\tilde{g}(\zeta)$, appearing in equation (27). This function includes terms representing heat transport due to convection as well as the thermal expansion effect. First, we note that thermal expansion is most pronounced near the bottom of the system, where the temperature increases most rapidly; second, the vapor and liquid volumetric fluxes are in
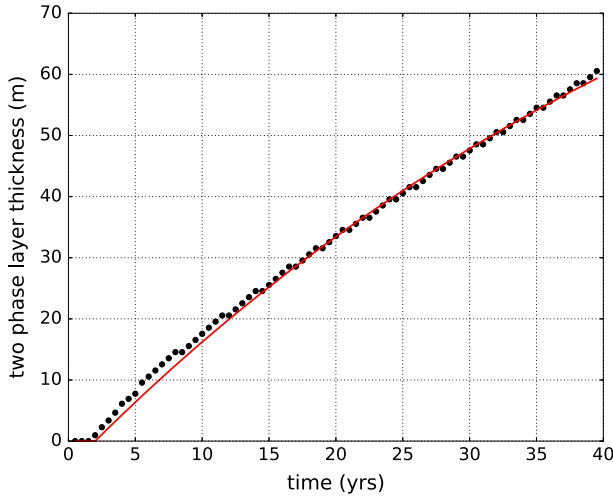
Fig. 11 Solution, $y_{23}(t)$, of Eq. (45) (*solid red curve*) is plotted over simulated values (*black dots*) for the height of the interface between the two-phase zone and the overlying single-phase fluid

opposite directions in the two-phase zone, approximately balancing one another at the y_{23} interface. With these considerations in mind, we parameterize $\tilde{g}(\zeta)$ as

$$\tilde{g}(\zeta) = S(1 - \zeta)^n, \tag{60}$$

where S and n are dimensionless constants. Finally, we note that the temperature at y_{23} varies slightly as the interface moves upward because the pressure decreases and lowers the temperature of phase transition. To include this effect, we use the linear formula

$$T_{23}(t) = \left[\frac{T_{23,f} - T_{23,i}}{t_f - t_i} \right] (t - t_i) + T_{23,i}, \tag{61}$$

where the subscript i denotes initial values and the subscript f denotes final values. We take 10 years as the initial time and 40 years as the final time. With equation (61) and the above values of S and n (given in Table 1), analytical temperatures are plotted against the numerically simulated temperatures in Fig. 12.

5 Discussion

5.1 Brine Sequestration

From the brine layer model of Sect. 3.1 and 4.1, we derive and discuss an expression for the quasi-steady-state brine layer thickness. Setting $dy_{12}/dt = 0$ in equation (40) and solving for $y_{12}(t \to \infty) \equiv y_{12,\infty}$ gives

$$y_{12,\infty} = \frac{\gamma}{\eta} = \frac{(\rho_1 v_1 X_1)_{12}}{\phi \frac{d}{dt} \langle \rho_1 X_1 \rangle}, \tag{62}$$

where the numerator is evaluated at the top of the brine layer, while the angle brackets indicate averaging over the entire layer. We note that, although y_{12} no longer increases with time,
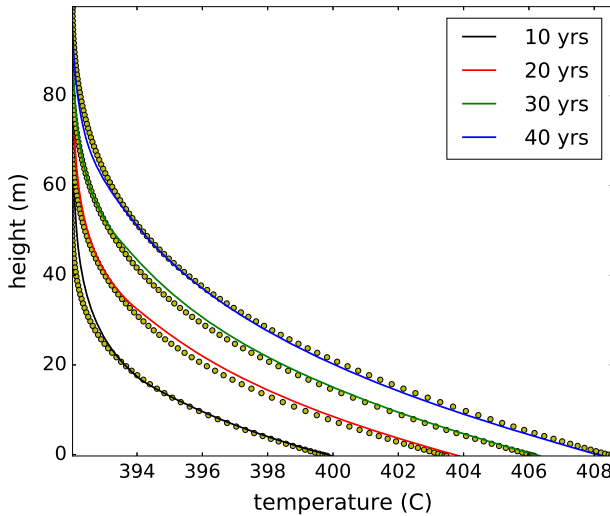
Fig. 12 Temperatures derived from an analytical model (*solid curves*) are plotted over those derived from a numerical simulation (*yellow dots*)

the salt content of the brine layer does, hence the presence of time derivative term in the denominator. The presence of this term suggests why the steady state is only approximate or "quasi": The salinity in the layer will increase until the dynamics of the system changes and the balance expressed by (40) is no longer applicable.

As the salinity increases, eventually either halite will precipitate or the effect of diffusion, which we have so far neglected, will become important. We may estimate the salinity at which diffusion becomes important by considering the case in which salt diffusion out of the top of the brine layer balances salt delivered into the top via advection. This balance is expressed as

$$\frac{\partial}{\partial y}(\rho_l v_l X_1) = D\phi\rho_l \frac{\partial^2 X_1}{\partial y^2}, \tag{63}$$

where D is the salt diffusivity. Because the brine forms a boundary layer, we may make the approximation

$$\frac{\partial}{\partial y}(\rho_l v_l X_1) \approx \frac{\Delta(\rho_l v_l X_1)}{\Delta y} = \frac{(\rho_l v_l X_1)_{\text{top}} - (\rho_l v_l X_1)_0}{y_{12,\infty} - 0} = \frac{(\rho_l v_l X_1)_{12}}{y_{12,\infty}}, \tag{64}$$

where the last equation follows because the volumetric flux at the bottom boundary of the system vanishes. Similarly,

$$D\phi\rho_l \frac{\partial^2 X_1}{\partial y^2} \approx D\phi\rho_l \frac{\Delta X_1}{y_{12,\infty}^2}, \tag{65}$$

where ΔX_1 is the increase in salinity from the top to the bottom of the brine layer. Substituting (64) and (65) into (63) yields

$$\Delta X_1 \approx \frac{(v_l X_1)_{12} y_{12,\infty}}{D\phi}. \tag{66}$$

Substituting values of these quantities from the simulation of Sect. 4 yields $\Delta X_1 \approx 60\,\text{wt\%}$ NaCl; halite precipitation would start to occur well before achieving this threshold.

Equation (62) suggests that increasing the permeability, and hence the volumetric flux, may increase the thickness of the quasi-steady-state brine layer. Complicating matters is the fact that the $d\langle \rho_1 X_1 \rangle / dt$ and $(\rho_1 v_1 X_1)_{\text{top}}$ are not independent—more salt entering the top contributes to faster buildup of salt within the layer. Nevertheless, increasing the permeability does increase the thickness of the brine layer, as a simulation with increased permeability compared to that in Sect. 4 ($10^{-14}\,\text{m}^2$, compared to $10^{-15}\,\text{m}^2$) showed an increase in thickness of the layer (4.8 m, compared to 2.3 m).

We consider the possibility of allowing brine to flow laterally out the sides of the heat pipe, which may more closely approximate brine sequestration in an actual hydrothermal system. Consider a segment of the pipe with vertical extent Δy, centered around a height y within the brine layer. We assume that the amount of brine, ΔQ, leaving this segment is proportional to $y_{12} - y$ (i.e., the distance from the top of the brine layer), the amount of time Δt that has passed, and the exposed surface area of the segment, $\Delta \sigma$:

$$\Delta Q = q(y_{12} - y)\Delta \sigma \, \Delta t, \tag{67}$$

where q is a constant. The surface area is given by

$$\Delta \sigma = 2\Delta y(\Delta x + \Delta z), \tag{68}$$

where Δx is the width of the front of the pipe and Δz is the width of the side. Defining the circumference of the pipe as $\tilde{\sigma} \equiv 2(\Delta x + \Delta z)$, the salt lost from the sides of the entire brine layer is

$$Q = \Delta t q \tilde{\sigma} \int_0^{y_{12}} (y_{12} - y)\mathrm{d}y = \frac{q}{2}\Delta t \tilde{\sigma} y_{12}^2. \tag{69}$$

Incorporating the sink term (69) and making the appropriate replacements for $\mathcal{F}$ and $\mathcal{C}$ (see Sect. 3.1), equation (9) becomes

$$\frac{1}{A}\frac{\mathrm{d}I}{\mathrm{d}t} = (\rho_1 v_1 X_1)_{12} + \phi(\rho X)_{12}\frac{\mathrm{d}y_{12}}{\mathrm{d}t} - \frac{q}{2}\left(\frac{\tilde{\sigma}}{A}\right)y_{12}^2. \tag{70}$$

Following the same steps as in the derivation of equation (40), and using the abbreviation $\xi \equiv \rho X$, the resulting equation is

$$\frac{\mathrm{d}y_{12}}{\mathrm{d}t}(\langle \xi \rangle - \xi_{12}) + y_{12}\frac{\mathrm{d}\langle \xi \rangle}{\mathrm{d}t} = \left(\xi_1 \frac{v_1}{\phi}\right)_{12} - \frac{q}{2}\left(\frac{\tilde{\sigma}}{\phi A}\right)y_{12}^2. \tag{71}$$

Setting the time derivative to zero and rearranging yields

$$\frac{q}{2}\left(\frac{\tilde{\sigma}}{\phi A}\right)y_{12,\infty}^2 + y_{12,\infty}\frac{\mathrm{d}}{\mathrm{d}t}\langle \xi \rangle - \left(\frac{\xi_1 v_1}{\phi}\right)_{12} = 0. \tag{72}$$

This equation can be solved via the quadratic formula; however, if the amount of lateral salt loss is small, the solution can be expressed perhaps more informatively as a series of corrections to (62) as follows.

It is first necessary to non-dimensionalize (72) so that the magnitudes of the coefficients can be meaningfully compared. A dimensionless height may be defined as

$$\zeta = \frac{y_{12,\infty}}{(\xi_1 v_1)_{12}}\phi \frac{\mathrm{d}}{\mathrm{d}t}\langle \xi \rangle, \tag{73}$$

and then (72) may be expressed as

$$\frac{q}{2}\left(\frac{\tilde{\sigma}}{\phi A}\right)\left[\frac{(\xi_l v_l)_{12}}{\phi\left(\frac{d}{dt}\langle\xi\rangle\right)^2}\right]\zeta^2 + \zeta - 1 = 0. \tag{74}$$

Define the coefficient of ζ^2 as ϵ and suppose it is small compared to unity. Then the solution to (74) can be expanded in a perturbative series as

$$\zeta = \zeta_0 + \epsilon\zeta_1 + \epsilon^2\zeta_2\cdots, \tag{75}$$

where the ζ_i are successive approximations to ζ. Putting (75) into (74) and keeping terms to the first order in ϵ gives

$$\epsilon(\zeta_0^2 + \zeta_1) + (\zeta_0 - 1) = 0. \tag{76}$$

Setting coefficients of differing powers of ϵ to zero yields the solution

$$\zeta = 1 - \epsilon, \tag{77}$$

which is the same as

$$y_{12,\infty} = \frac{\gamma}{\eta}\left[1 - \frac{q}{2}\left(\frac{\tilde{\sigma}}{\phi A}\right)\left(\frac{\gamma}{\eta}\right)\left(\frac{1}{\frac{d}{dt}\langle\xi\rangle}\right)\right] \tag{78}$$

We note the presence of the geometrical factor $\tilde{\sigma}/\phi A$ in the correction term. If the cross section is increased, for example, the overall effect is to lower the magnitude of this factor and hence also of the correction term.

5.2 Energy Balance

In deriving equation (45), we integrated the equation expressing energy balance from the bottom of the system to the height of the two-phase layer; we now consider how each term in the equation contributes to the energy balance within the layer. The energy balance (48) can be expressed as

$$(1-\phi)\rho_r c_{pr}\frac{\partial T}{\partial t} + \phi\rho\frac{\partial h}{\partial t} + \phi h\frac{\partial\rho}{\partial t} + \frac{\partial}{\partial y}(\rho_l v_l h_l + \rho_v v_v h_v) = \tilde{\lambda}\frac{\partial^2 T}{\partial y^2} = -\frac{\partial}{\partial y}\mathcal{F}_c, \tag{79}$$

where we have defined the conductive flux as $\mathcal{F}_c = -\tilde{\lambda}\frac{\partial T}{\partial y}$. The term $\phi h\partial\rho/\partial t$ is negative due to thermal expansion, which also induces mass and heat fluxes across the y_{23} interface. To consider these fluxes explicitly, we note that, according to the mass continuity equation,

$$\phi\frac{\partial\rho}{\partial t} = -\frac{\partial}{\partial y}(\rho_l v_l + \rho_v v_v). \tag{80}$$

Substituting this equation into (79) and rearranging gives

$$(1-\phi)\rho_r c_{pr}\frac{\partial T}{\partial t} + \phi\rho\frac{\partial h}{\partial t} = h\frac{\partial}{\partial y}(\rho_l v_l + \rho_v v_v) - \frac{\partial}{\partial y}(\rho_l v_l h_l + \rho_v v_v h_v) - \frac{\partial}{\partial y}\mathcal{F}_c. \tag{81}$$

Integrating the above equation from $y = 0$ to $y = y_{23}$ yields

$$(1 - \phi)\rho_r c_{\text{pr}} \int_0^{y_{23}} \frac{\partial T}{\partial t} dy + \phi \int_0^{y_{23}} \rho \frac{\partial h}{\partial t} dy$$
$$= \int_0^{y_{23}} h \frac{\partial}{\partial y}(\rho_l v_l + \rho_v v_v) dy - (\rho_l v_l h_l + \rho_v v_v h_v)_{23} - \mathcal{F}_{c,23} + \mathcal{F}_0, \qquad (82)$$

where $\mathcal{F}_0$ is the applied flux at the bottom boundary of the system. By the second mean value theorem for integrals, there exists a point y_b between $y = 0$ and $y = y_{23}$ such that

$$\int_0^{y_{23}} h \frac{\partial}{\partial y}(\rho_l v_l + \rho_v v_v) dy = h(y_b) \int_0^{y_{23}} \frac{\partial}{\partial y}(\rho_l v_l + \rho_v v_v) dy. \qquad (83)$$

If we define $h(y_b) = h_b$, we can therefore write (82) as

$$(1 - \phi)\rho_r c_{\text{pr}} \int_0^{y_{23}} \frac{\partial T}{\partial t} dy + \phi \int_0^{y_{23}} \rho \frac{\partial h}{\partial t} dy$$
$$= h_b(\rho_l v_l + \rho_v v_v)_{23} - (\rho_l v_l h_l + \rho_v v_v h_v)_{23} - \mathcal{F}_{c,23} + \mathcal{F}_0. \qquad (84)$$

As long as it is remembered that h_b is a constant, this equation may be expressed as

$$(1 - \phi)\rho_r c_{\text{pr}} \int_0^{y_{23}} \frac{\partial T}{\partial t} dy + \phi \int_0^{y_{23}} \rho \frac{\partial h}{\partial t} dy = [\rho_l v_l (h_b - h_l) + \rho_v v_v (h_b - h_v)]_{23}$$
$$- \mathcal{F}_{c,23} + \mathcal{F}_0. \qquad (85)$$

Both terms on the left-hand side of (85) are positive, because both the rock and fluid gain energy as the column is heated from below; therefore, the right-hand side must also be positive. If we had not considered the expansion effect explicitly and had instead employed the term $\phi \frac{\partial(h\rho)}{\partial t}$ in equation (79), this term could be negative (and indeed is, in the simulation discussed in section (4)), even though both rock and fluid gain energy with time. We would have instead obtained

$$(1 - \phi)\rho_r c_{\text{pr}} \int_0^{y_{23}} \frac{\partial T}{\partial t} dy + \phi \int_0^{y_{23}} \frac{\partial(\rho h)}{\partial t} dy$$
$$= -[\rho_l v_l h_l + \rho_v v_v h_v]_{23} - \mathcal{F}_{c,23} + \mathcal{F}_0, \qquad (86)$$

and then both sides of the above equation can turn out to be negative when there is strong thermal expansion, the negative right hand giving the impression that more energy is being transferred from the top of the two-phase layer than is being delivered at the bottom. Equation (85) makes manifest that such is not the case.

5.3 Using the Framework Without a Numerical Model

When we employed the extended Stefan method to study the heat pipe, we relied on a numerical simulation to supply the functional forms of certain key quantities; in this section, we indicate how the method might be used in the absence of simulation output. The most difficult part of the Stefan problem is finding the position of the advancing phase interfaces as functions of time. Consider the problem, from Sect. 3.1, of finding the brine interface position $y_{12}(t)$. To form the governing equation for y_{12}, we require specific forms for the functions η and γ from equations (41) and (42). In the absence of numerical results, the variables appearing in these functions must be supplied by a separate analytic model; which model that is depends on the context. The method presented here may be thought of as a general framework requiring specific models as inputs. For example, suppose liquid velocity

is given from a buoyancy-driven flow model, that the thermodynamic quantities within the brine layer are constants, and that the average salt content of the brine layer is constant. The second of these assumptions leads to $\eta = 0$, while the first leads to

$$v_l = \frac{kg}{\mu_l}(\rho - \rho_l), \tag{87}$$

which in turn gives $\gamma = const$. In this situation, the solution for the interface position is $y_{12}(t) = \gamma t$. Such a model could be appropriate for very early times (see Fig. 8 between $t = 2$ and $t = 4$ years).

6 Conclusion

We have presented a framework that extends the classical Stefan-type solution method to deal with multi-component, multi-phase 1D porous flows that involve distinct propagating interfaces. Once the partial differential equations governing solute and energy balance have been provided, these equations may be converted into ordinary differential equations whose solutions give the positions of the corresponding interfaces as functions of time. By splitting the solution domain into pieces and considering the interfaces as moving boundaries, the temperature profile for the whole domain may be obtained. We have illustrated this framework via application to the 1D saltwater heat pipe.

The dynamics of the heat pipe system are far from trivial. Neither the interface between the brine and two-phase zones nor that between the two-phase and single-phase zones evolve according to any simple prescription, such as linearly with time or as $(time)^{1/2}$. Fluid advection must be accounted for in all regions, even with a relatively low permeability, such as that in the numerical simulation used for comparison with the analytical models. Large variations in thermodynamic properties and fluid velocities must be taken into account in the two-phase zone; volumetric fluxes in the two-phase zone are not given by any simple approach such as a purely buoyancy-driven model.

Even though the salinity is constant at the top of brine zone, the layer stops growing after short time; this halt in growth occurs because the salt content of the layer continues to increase with time while the effect of salt diffusion is small compared to that of salt advection. The increase in salt content is due to downward liquid salt flux at top of brine zone, with negligible salt carried across the interface by vapor. Pipe geometry is important for the ability of a system to store brine. For example, in a simple model, increasing the pipe circumference decreases the amount of salt loss from the sides of the pipe.

In contrast to the brine layer, for the two-phase zone increased heat input initiates a phase change and conduction is strong even compared to the advection of heat by the vapor phase. The result is that the two-phase interface grows nearly linearly, but departs from linearity because transport of heat across the top of the layer is not constant in time. Thermal expansion is non-negligible, and in such a case it is conceptually advantageous to rewrite the energy balance over the two-phase region as in (85), because this form makes the fact of energy conservation evident.

Appendix 1: Alternative Derivation of Equation (12)

The equations expressing the balance of salt or heat can both be cast in the form

$$\frac{\partial \mathcal{C}}{\partial t} + \frac{\partial \mathcal{F}}{\partial y} = 0, \tag{88}$$

where $\mathcal{C}$ represents the content of salt or energy and $\mathcal{F}$ represents combined advective and diffusive fluxes. Integrating both sides from the bottom to the top of the expansion layer gives

$$\int_0^{y_{ij}} \frac{d\mathcal{C}}{dt} dy = \mathcal{F}_0 - \mathcal{F}_{ij} \equiv \mathcal{F}. \tag{89}$$

According to the Leibniz integral theorem,

$$\frac{d}{dt} \int_0^{y_{ij}} \mathcal{C} dy = \int_0^{y_{ij}} \frac{\partial \mathcal{C}}{\partial t} dy + \mathcal{C}(y_{ij}, t) \frac{dy_{ij}}{dt}. \tag{90}$$

Solving for the first term on the right-hand side and substituting the result into (89) gives

$$\frac{d}{dt} \int_0^{y_{ij}} \mathcal{C} dy - \mathcal{C}_{ij} \frac{dy_{ij}}{dt} = \mathcal{F}, \tag{91}$$

where $\mathcal{C}_{ij} \equiv \mathcal{C}(y_{ij}, t)$. Defining the average content density as in equation (10) and substituting into the above equation leads to equation (12).

Appendix 2: Derivation of the Stefan Condition

In the original Stefan problem that involves a half plane filled with melting ice, the position of the melt interface is found by imposing the Stefan condition [see (Carslaw and Jaeger 1959], pg. 284); in this section, we show how this condition may be derived from equation (12). Consider the upper half plane ($y \geq 0$) filled with ice and heated from below. In our notation, the Stefan condition reads

$$\lambda_2 \frac{\partial T_2}{\partial y} - \lambda_1 \frac{\partial T_1}{\partial y} = L\rho \frac{dy_{12}}{dt}, \tag{92}$$

where the subscript 1 refers to liquid, the subscript 2 refers to ice, and L is the latent heat of fusion. In this scenario, equation (12) becomes

$$\rho \frac{dy_{12}}{dt} [\langle h \rangle - h_{12}] + \rho y_{12} \frac{d}{dt} \langle h \rangle = \mathcal{F}_0 - \mathcal{F}_{12}, \tag{93}$$

where ρ is the liquid density, h is the liquid enthalpy, and we have made the replacement $\mathcal{C} = \rho h$. For simplicity, we have assumed that the liquid is raised only slightly above freezing so that variation of density within the liquid phase may be neglected. First, we note that the heat flux into the y_{12} interface from below is equal to the flux at the bottom boundary of the system minus the portion of that heat absorbed by the layer of liquid between the bottom boundary and y_{12}; mathematically, this statement translates to

$$\mathcal{F}_{12,-} = \mathcal{F}_0 - \rho y_{12} \frac{d}{dt} \langle h \rangle. \tag{94}$$

Second, we relabel the quantity $\mathcal{F}_{12}$ as $\mathcal{F}_{12,+}$, emphasizing that it is the flux of heat upward from y_{12}. Making these replacements and setting

$$\langle h \rangle - h_{12} = L \tag{95}$$

in equation (93) yields

$$L\rho \frac{dy_{12}}{dt} = \mathcal{F}_{12,-} - \mathcal{F}_{12,+}. \tag{96}$$

Using Fourier's law of heat conduction, we write

$$\mathcal{F}_{12,-} = -\lambda_1 \frac{\partial T_1}{\partial y}, \tag{97}$$

and

$$\mathcal{F}_{12,+} = -\lambda_2 \frac{\partial T_2}{\partial y}, \tag{98}$$

where both derivatives are evaluated at y_{12}. Substituting these expressions into (96) gives equation (92).

In the problem of the receding ice sheet, the classical Stefan condition can be used to find the form of $y_{12}(t)$ together with the temperature profile; however, this technique only works under very restricted conditions. For example, imposing a heat flux condition at the bottom boundary of the system instead of a constant temperature condition already leads to problems (see (Carslaw and Jaeger 1959)) for details). The generalized condition (12) avoids this difficulty by representing $y_{ij}(t)$ as the solution of its own differential equation instead of as an auxiliary quantity to be determined simultaneously with $T(y, t)$.

Appendix 3: Derivation of Condition (20)

Using the definitions

$$T = Fy_{ij}\theta + T_{ij} + F(y_{ij} - y), \tag{99}$$

and

$$\tau = \frac{\kappa_i t}{y_{ij}^2}, \tag{100}$$

we find that

$$\frac{1}{F} \frac{\partial T}{\partial t} = \dot{y}_{ij}(\theta + 1) + \frac{\kappa_i}{y_{ij}} \frac{\partial \theta}{\partial \tau} - 2\tau \dot{y}_{ij} \frac{\partial \theta}{\partial \tau}. \tag{101}$$

We seek the condition under which the second term on the right-hand side of (101) dominates the first and the third terms. The first and third terms are both of the order $\dot{y}_{ij}$, while the second term is of order κ_i / y_{ij}. Hence, the desired condition is that

$$\dot{y}_{ij} \ll \frac{\kappa_i}{y_{ij}}, \tag{102}$$

which is identical with (20). This condition is sufficient but not necessary, because the first and third terms on the right-hand side of (101) are of opposite sign, and so may approximately cancel one another even if (102) is not satisfied.

Appendix 4: Derivation of Propagator and Green's Function

To solve for $\theta_{\mathrm{H}}(\zeta, \tau)$ and construct the propagator, we begin by finding the eigenfunctions $\psi_n(\zeta)$ and eigenvalues λ_n satisfying

$$-\frac{\mathrm{d}^2}{\mathrm{d}\theta^2}\psi_n(\zeta) = \lambda_n\psi_n(\zeta), \tag{103}$$

where the eigenfunctions are required to satisfy the homogeneous boundary conditions (22) and (23). The solutions, normalized on the interval $0 \leq \zeta \leq 1$, are

$$\psi_n(\zeta) = \sqrt{2}\cos(\sqrt{\lambda_n}\zeta), \tag{104}$$

with

$$\lambda_n = \left[\frac{(2n+1)\pi}{2}\right]^2, \tag{105}$$

and $n \in \mathbb{N}$. Now we search for a solution of the form

$$\theta_{\mathrm{H}}(\zeta, \tau) = \sum_{n=0}^{\infty} a_n(\tau)\psi_n(\zeta), \tag{106}$$

where the time-dependent coefficients $a_n(\tau)$ are to be determined. Substituting (106) into (21), setting $\tilde{f}(\zeta) = 0$, and keeping in mind that the ψ_n satisfy (103), we obtain

$$\sum_{n=0}^{\infty} \psi_n\left(\frac{\mathrm{d}a_n}{\mathrm{d}\tau} + \lambda_n a_n\right) = 0. \tag{107}$$

The eigenfunctions are all linearly independent, so the only way the above equation can be satisfied is if each coefficient of ψ_n vanishes; the resulting differential equation in $a_n(\tau)$ has the solution

$$a_n(\tau) = A_n e^{-\lambda_n \tau}, \tag{108}$$

where A_n is a constant for each n. Equation (106) now takes the form

$$\theta_{\mathrm{H}}(\zeta, \tau) = \sum_{n=0}^{\infty} A_n e^{-\lambda \tau}\psi_n(\zeta). \tag{109}$$

It remains to choose the constants A_n so that the initial condition (24) is satisfied. Applying the initial condition to (109) gives

$$\theta_{\mathrm{H}}(\zeta, 0) = \sum_{n=0}^{\infty} A_n\psi_n(\zeta). \tag{110}$$

Multiplying both sides of this equation by $\psi_m(\zeta)$, integrating from 0 to 1, and keeping in mind the orthonormality of the eigenfunctions results in

$$A_m = \int_0^1 \theta(\zeta', 0)\psi_m(\zeta')\mathrm{d}\zeta'. \tag{111}$$

Changing m back to n, substituting the above expression into (109), and rearranging give the solution to the homogeneous problem as

$$\theta_{\mathrm{H}}(\zeta, \tau) = \int_0^1 \left[\sum_{n=0}^{n=\infty} \psi_n(\zeta')\psi_n(\zeta)e^{-\lambda_n \tau}\right]\theta(\zeta', 0)\mathrm{d}\zeta'. \tag{112}$$

The expression in brackets is the kernel of the desired integral operator, which propagates the solution at $\tau = 0$ to that at a later time τ. Therefore, the kernel that propagates a solution at $\tau = \tau'$ to a later time τ is

$$\mathcal{P}(\zeta, \zeta', \tau, \tau') = \sum_{n=0}^{\infty} \psi_n(\zeta')\psi_n(\zeta)e^{-\lambda_n(\tau-\tau')}. \tag{113}$$

It can be shown that multiplying the propagator with the Heaviside step function $H(\tau - \tau')$ produces the Green function required for solution of the associated inhomogeneous problem (see Bayin 2006); hence, the desired Green function is

$$\mathcal{G}(\zeta, \zeta', \tau, \tau') = \mathcal{P}(\zeta, \zeta', \tau, \tau')H(\tau - \tau'). \tag{114}$$

The solution to the inhomogeneous problem is then

$$\theta_{\mathrm{I}}(\zeta, \tau) = \int_0^{\infty} \int_0^1 \mathcal{G}(\zeta, \zeta', \tau, \tau')\tilde{g}(\zeta')\mathrm{d}\zeta' d\tau'. \tag{115}$$

Carrying out the integral as far as possible with general $\tilde{g}(\zeta')$ results in

$$\begin{aligned}
\theta_{\mathrm{I}}(\zeta, \tau) &= \sum_{n=0}^{\infty} \psi_n(\zeta') \int_0^1 \psi_n(\zeta')\tilde{g}(\zeta')\mathrm{d}\zeta' \int_0^{\tau} e^{-\lambda_n(\tau-\tau')}d\tau' \\
&= \sum_{n=0}^{\infty} \frac{1 - e^{-\lambda_n \tau}}{\lambda_n}\psi_n(\zeta) \int_0^1 \psi_n(\zeta')\tilde{g}(\zeta')\mathrm{d}\zeta',
\end{aligned} \tag{116}$$

which is the same as equation (27). Using equation (24) and completing the integral in (112) yields

$$\theta_{\mathrm{H}}(\zeta, \tau) = \sum_{n=0}^{\infty} \frac{\sqrt{2}}{\lambda_n}e^{-\lambda_n \tau}\psi_n(\zeta), \tag{117}$$

which is the same as equation (26). The full dimensionless solution $\theta(\zeta, \tau)$ is now given by (25).

References

Bai, W., Xu, W., Lowell, R.P.: The dynamics of submarine geothermal heat pipes. Geophys. Res. Lett. (2003). doi:10.1029/2002GL016176

Bayin, S.: Mathematical Methods in Science and Engineering. Wiley-Interscience, Hoboken (2006)

Berndt, M., Seyfried Jr., W.: Boron, bromine, and other trace elements as clues to the fate of chlorine in mid-ocean ridge vent fluids. Geochim. Cosmochim. Acta **54**, 2235–2245 (1990)

Carslaw, H.S., Jaeger, J.C.: Conduction of Heat in Solids. Clarendon Press, Oxford (1959)

Choi, J., Lowell, R.P.: The response of two-phase hydrothermal systems to changing magmatic heat input at mid-ocean ridges. Deep Sea Res. **II**(121), 17–30 (2015)

Corliss, J.B., Dymond, J., Gordon, L.I., Edmund, J.M., Von Herzen, R.P., Ballard, R.D., Green, K., Williams, D., Bainbridge, A., Crane, K., Van Andel, T.H.: Submarine thermal springs on the Galapagos Rift. Science **203**, 1073–1089 (1979)

Elderfield, H., Schultz, A.: Mid-ocean ridge hydrothermal fluxes and the chemical composition of the ocean. Ann. Rev. Earth Planet. Sci. **24**, 191–224 (1996)

Han, L., Lowell, R.P., Lewis, K.C.: Dynamics of two-phase hydrothermal systems at a surface pressure of 25 mPa. J. Geophys. Res. **118**, 2635–2647 (2013). doi:10.1002/jgrb.50158

Hessler, R.R., Kaharl, V.A.: The Deep-Sea Hydrothermal Vent Community: An Overview, Volume 91 of Geophysical Monograph Series. AGU, Washington (1995)

Lewis, K.C.: Forgotten merits of the analytic viewpoint. EOS **94**, 71–72 (2013)

Lewis, K.C., Lowell, R.P.: Numerical modeling of two-phase flow in the NaCl-H$_2$O system I: introduction of a numerical method and benchmarking. J. Geophys. Res. (2009a). doi:10.1029/2008JB006029

Lewis, K.C., Lowell, R.P.: Numerical modeling of two-phase flow in the NaCl-H$_2$O system II: applications. J. Geophys. Res. (2009b). doi:10.1029/2008JB006030

Lewis, K.C., Zyvoloski, G.A., Travis, B., Wilson, C., Rowland, J.: Drainage subsidence associated with arctic permafrost degradation. J. Geophys. Res. (2012). doi:10.1029/2011JF002284

Lewis, K.C., Karra, S., Kelkar, S.: A model for tracking fronts of stress induced permeability enhancement. Transp. Porous Media **99**, 17–35 (2013)

Lowell, R.P., Houghton, J.L., Farough, A., Craft, K.L., Larson, B.I., Miele, C.D.: Mathematical modeling of diffuse flow in seafloor hydrothermal systems: the potential extent of the subsurface biosphere at mid-ocean ridges. Earth Planet. Sci. Lett. **425**, 145–153 (2015). doi:10.1016/j.epsl.2015.05.047

McGuinness, M.J.: Heat pipe stability in geothermal reservoirs. Trans. Geotherm. Resourc. Counc. **14**, 1301–1307 (1990)

McGuinness, M.J.: Steady solution selection and existence in geothermal heat pipes—1. The convective case. Int. J. Heat Mass Transf. **39**, 259–274 (1996)

Preuss, K.: A quantitative model of vapor dominated geothermal reservoirs as heat pipes in fractured porous rocks. Trans. Geotherm. Resour. Counc. **9**, 353–361 (1985)

Singh, S., Lowell, R.P., Lewis, K.C.: Numerical modeling of phase separation at the Main Endeavour Field, Juan de Fuca Ridge. Geochem. Geophys. Geosyst. **14**, 4021–4034 (2013). doi:10.1002/ggge.20249

Stauffer, P.H., Lewis, K.C., Stein, J.S., Travis, B.J., Lichtner, P., Zyvoloski, G.: Joule–Thomson effects on the flow of liquid water. Transp. Porous Media **105**, 471–485 (2014)

Steele-MacInnis, M.J., Han, L., Lowell, R.P., Rimstidt, J.D., Bodnar, R.J.: Quartz precipitation and fluid-inclusion characteristics in sub-seafloor hydrothermal systems associated with volcanogenic massive sulfide deposits. Cent. Eur. J. Geosci. (2012a). doi:10.2478/s13533-011-0053-z

Steele-MacInnis, M.J., Han, L., Lowell, R.P., Rimstidt, J.D., Bodnar, R.J.: The role of fluid phase immiscibility in quartz precipitation and dissolution in sub-seafloor hydrothermal systems. Earth Planet. Sci. Lett. **321–322**, 139–151 (2012b)

Stein, C.A., Stein, S.: Heat Flow and Hydrothermal Circulation, Volume 91 of Geophysical Monograph Series. AGU, Washington (1995)

Straus, J., Schubert, G.: One-dimensional model of vapor-dominated geothermal systems. J. Geophys. Res. **86**, 9433–9438 (1981)

Von Damm, K.: Evolution of the Hydrothermal System at East Pacific Rise 9°50'N: Geochemical Evidence for Changes in the Upper Oceanic Crust, Volume 148 of Geophysical Monograph Series. AGU, Washington (2004)

Von Damm, K., Buttermore, L., Oosting, S., Bray, A., Fornari, D., Lilley, M., Shanks Jr., W.S.: Direct observation of the evolution of a seafloor "black smoker" from vapor to brine. Earth Planet. Sci. Lett. **149**, 101–111 (1997)

Von Damm, K., Parker, C., Gallant, R., Loveless, J.: Chemical evolution of hydrothermal fluids from epr 21°N: 23 years later in a phase separating world. Eos Transactions of AGU, 83. Fall meeting supplement, Abstract V61B-1365 (2002)

Xu, W., Lowell, R.P.: Oscillatory instability of one-dimensional two-phase hydrothermal flow in heterogeneous porous media. J. Geophys. Res. **103**, 20859–20868 (1998)

Young, R.: Phase transitions in one-dimensional steady state hydrothermal flows. J. Geophys. Res. **101**, 18011–18022 (1996)